ARTICLE

Polyelectrolyte/Nanosilicate Thin-Film Assemblies: Influence of pH on Growth, Mechanical Behavior, and Flammability

Yu-Chin Li, Jessica Schulz, and Jaime C. Grunlan*

Department of Mechanical Engineering, Texas A&M University, College Station, Texas 77843

ABSTRACT Thin composite films of branched polyethylenimine (BPEI) and Laponite clay platelets were prepared using layer-by-layer assembly. The film thickness was tailored by altering the pH of the aqueous mixtures used to deposit these films, resulting in growth that ranged from 0.5 to 5 nm/bilayer (BL). High-pH BPEI and low-pH clay produced the thickest films. The microstructure of tilted Laponite clay platelet stacks is observed with transmission electron microscopy when using unadjusted BPEI (pH 10.3) and pH 6 Laponite. This recipe resulted in a film with 83 wt % clay and a hardness of 0.5 GPa. In all films, the clay platelets are uniformly deposited and look analogous to a cobblestone path in atomic force microscopy surface images. Several 40-BL films, with thicknesses of 100 nm or more, exhibit reduced moduli ranging from 7 to 10 GPa and hardness of around 0.5 GPa, suggesting that these transparent films could be useful as hard coatings for plastic films. These thin coatings were also deposited onto cotton fabric. Each individual cotton fiber was uniformly coated, and the fabric has significantly more char left after burning than the uncoated fabric. Thermogravimetric analysis results reveal that fabric coated with 10 BLs of BPEI/Laponite produces up to 6 wt % char at 500 °C, which is almost 1 order of magnitude greater than that of untreated fabric. This initial study demonstrates that polymer/clay assemblies could improve the thermal stability of cotton and may be useful for fire safety applications.

KEYWORDS: layer-by-layer assembly • clay • TEM • nanocomposites • flame suppression

INTRODUCTION

Layer-by-layer (LbL) assembly has become a popular method to fabricate multifunctional films that are typically less than 1 μm thick (1−3). These thin films are assembled by alternating the deposition of positively and negatively charged layers on a substrate. Deposition often involves the soaking of a charged (or at least polar) substrate in aqueous mixtures of charged polymers and/or particles, alternating between cationic and anionic species. The primary means of multilayer buildup is electrostatic attractions, but a variety of other interactions have been successfully exploited. For example, assemblies have been built through donor/acceptor interactions (4−6), hydrogen bonding (7, 8), and covalent bonds (9, 10). In the case of electrostatic growth, each pair of positively and negatively charged layers is referred to as a bilayer (BL). Typical BL thicknesses range from 1 to 100 nm, depending on factors that include chemistry (11), molecular weight (12), temperature (13, 14), counterions (15), ionic strength (16), and pH (14, 17). A variety of LbL-assembled functional thin films are currently being evaluated for properties that include antimicrobial (18, 19), antireflection (20), electrochromic (21−23), sensing (24−26), oxygen barrier (27), and biomedical applications (28). In many cases, solid nanoparticles, such as clay (27−31), are one type of the charged species imparting a desired property.

Smectite clays have been widely studied in LbL thin films, especially montmorillonite (MMT) (27, 32, 33) and Laponite (34−40). These platelet structures are a class of phyllosilicates, which exhibit swelling and exfoliation in water (29). Each individual clay platelet (elementary sheet) is composed of one central layer of Al^{3+} and Mg^{2+} octahedra, sandwiched between two layers of Si^{4+} tetrahedra. The thickness of these clay units is approximately 1 nm. They typically organize face-to-face into aggregates, but in aqueous dispersion, these faces become negatively charged as water intercalates and exfoliates the clay layers. At the edges, the clay elementary sheets contain many oxygen atoms and hydroxyl groups that can accept or release protons, depending on the pH of the suspension (29). Laponite is a synthetic clay with uniform disk-shaped particles that are approximately 25 nm in diameter (41, 42). Composite films of poly(diallyldimethylammonium chloride) (PDDA) and Laponite sorb water rapidly and reversibly, which led to their evaluation as humidity sensors (34). Additionally, modeling has indicated that PDDA/Laponite film formation results in significantly higher surface coverage than that of natural clay films (35). Film preparations with various Laponite contents (15−60 wt %) and poly(ethylene oxide) (PEO) have resulted in high degrees of orientation in both the polymer and clay platelets (37). Bulky, hydrophobic, and amphiphilic polyelectrolytes can be incorporated while still keeping the clay platelets aligned parallel to the substrate (38). Laponite, PEO, and linear polyethylenimine have also been used to form trilayers, whose anisotropic structure results in significant ion transport (40).

* Corresponding author. Tel: +1 979 845 3027. Fax: +1 979 862 3989. E-mail: jgrunlan@tamu.edu.

Received for review July 21, 2009 and accepted September 10, 2009

DOI: 10.1021/am900484q

Published on Web 09/25/2009

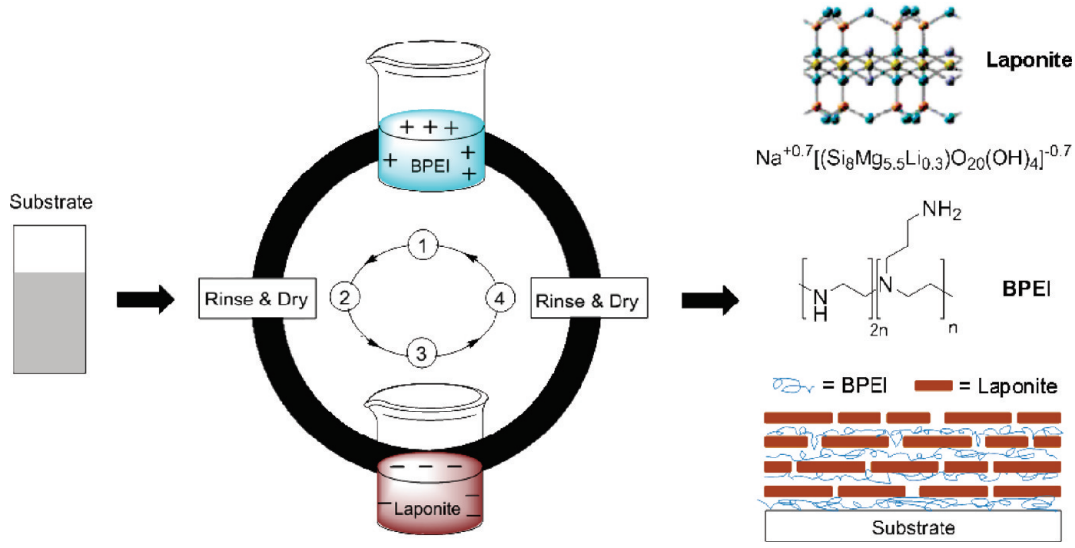

FIGURE 1. Schematic of the LbL deposition process used to prepare clay/BPEI assemblies. Steps 1−4 are repeated until the desired number of BLs are deposited.

In the present work, LbL assembly of branched polyethylenimine (BPEI) and Laponite clay is examined, with a focus on the influence of the pH of aqueous deposition mixtures, and the concentration of sodium chloride in the BPEI solution at a given pH, on the film growth, hardness, and antiflammability. The chemistry of both materials, along with the general deposition procedure, is shown in Figure 1. Quartz crystal microbalance (QCM) data indicate that the clay content in these films can be varied between 62 and 83 wt %, although no clear correlation between the clay content and the mechanical behavior is seen. Nanoindentation was performed on four different recipes to highlight the ability to tailor the mechanical behavior of these films with the pH, which may be useful in applications such as a scratch-resistant coatings for flexible electronics. Additionally, these clay-based assemblies impart flame-resistant behavior to cotton fabric by creating a protective sheath around each individual microfiber (∼10 μm diameter).

EXPERIMENTAL SECTION

Preparation of Deposition Solutions. Cationic deposition solutions were prepared by dissolving 0.1 wt % branched polyethylenimine (BPEI), with a molecular weight of 25 000 g/mol (Aldrich, Milwaukee, WI), into 18.2 MΩ deionized water from a Drect-QTM 5 Ultrapure Water System (Millipore, Bellerica, MA). The unadjusted pH of a 0.1 wt % BPEI solution is 10.3, but this value was adjusted to pH 7, 8, 9, and 10 by adding 1 M hydrochloric acid (36.5−38 % HCl; Mallinckrodt Chemicals, Phillipsburg, NJ). Synthetic Laponite RD clay (Southern Clay Product, Inc., Gonzales, TX) was exfoliated (0.2 wt %) in deionized water by simply adding it to water and slowly rolling it for 24 h to produce the anionic deposition mixtures. Laponite particles are disk-shaped, with an average diameter of 25 nm and a thickness of 0.96 nm (42). The faces of the Laponite disks are negatively charged in deionized water, and the cationic exchange capacity is about 55 mequiv/100 g. The unadjusted pH of a 0.2 wt % Laponite solution is 10.1, but this was adjusted to pH 6, 8, and 10 for depositions using 1 M HCl. The pH was measured with an Accumet Basic AB15 pH meter (Fisher Scientific, Pittsburgh, PA). Sodium chloride (reagent plus >99.5%, Aldrich) solutions of 1, 10, 100, and 1000 mM were prepared and used for the preparation of BPEI (at pH 8) and Laponite deposition solutions for different ionic strengths.

Substrates. Single-side-polished (100) silicon wafers (University Wafer, South Boston, MA) were used as deposition substrates for films characterized with ellipsometry, atomic force microscopy (AFM), scanning electron microscopy (SEM), and X-ray diffraction (XRD). In order to get good sections, transmission electron microscopy (TEM) imaging of these films required the use of a 125 μm polystyrene (PS) film (Goodfellow, Oakdale, PA) as the substrate for deposition. Prior to deposition, silicon wafers were rinsed with acetone and then deionized water and finally dried with filtered air. In the case of PS substrates, the film was rinsed with methanol and deionized water and dried with air. The clean PS substrates were then corona-treated with a BD-20C Corona Treater (Electro-Technic Products Inc., Chicago, IL) for 2 min. Corona treatment oxidizes the PS film surface and creates a negative surface charge (43, 44), which improves the adhesion of the first BPEI layer. Cotton fabric was supplied by the USDA Southern Regional Research Center (New Orleans, LA) and was coated and tested for flame retardancy.

LbL Film Deposition. All films were assembled on a given substrate using the procedure shown in Figure 1. The substrate was dipped into the ionic deposition solutions, alternating between BPEI (cationic) and Laponite (anionic), with each cycle corresponding to one BL. The first dip into each mixture was for 5 min, beginning with the cationic solution. Subsequent dips were for 1 min each. Every dip was followed by rinsing with deionized water for 30 s and drying with a stream of filtered air for 30 s. In the case of the fabrics, the drying step involved wringing out of the water instead of air-drying. After the desired BL numbers were achieved, the coated substrates were dried in the 70 °C oven for 15 min (except the fabrics, which were dried for 3 h).

Film Characterization. The film thickness was measured with a PHE-101 Discrete Wavelengh Ellipsometer (Microphotonics, Allentown, PA). The 632.8 nm laser was used at an incidence angle of 65°. A Maxtek Research QCM from Infinicon (East Syracuse, NY), with a frequency range of 3.8−6 MHz, was used in conjunction with 5 MHz quartz crystals to measure the weight per deposited layer. The crystal, in its holder, was dipped alternately into the positively and negatively charged solutions. Between each dip, the crystal, in the holder, was rinsed, dried, and left on the

microbalance for 5 min to stabilize. Cross sections of the clay/polymer assemblies were imaged with a JEOL 1200 EX transmission electron microscope (Mitaka, Tokyo, Japan), operated at 110 kV. Samples were prepared for imaging by embedding a piece of PS supporting the LbL film in epoxy and sectioning it with a microtome equipped with a diamond knife. Surface structures were imaged with a Nanosurf EasyScan 2 atomic force microscope (Nanoscience Instruments, Inc., Phoenix, AZ). AFM images were gathered in tapping mode with a XYNCHR cantilever tip. A Bruker AXS D8 Advanced Bragg−Brentano powder X-ray diffractometer (Cu Kα, $\lambda = 1.541$ Å; Bruker AXS Inc., Madison, WI) was used for both powder and glancing-angle XRD. Nanoindentation was performed by Hysitron, Inc. (Minneapolis, MN), using a TI-700 UBI nanomechanical test instrument to determine the hardness and reduced modulus of films on silicon with a diamond Cube-Corner indenter probe. A total of 15−20 indentation tests were performed on each sample. Each indent consisted of a 5 s loading segment, a 2 s hold segment, and a 5 s unloading segment. An indentation depth of 10 nm was used in most cases, which is the shallowest depth that can give reliable hardness and modulus values. Surface images of coated fabrics, as well as of the chars from fabrics (after direct exposure to a flame), were acquired with a Quanta 600 field-emission scanning electron microscope (FEI Co., Hillsboro, OR).

Thermal Analysis and Vertical Flame Test. The thermal stability of uncoated and coated fabrics was measured in a Q50 thermogravimetric analyzer (TA Instruments, New Castle, DE). Each sample was run under air from room temperature to 600 °C, at a heating rate of 20 °C/min. Vertical flame tests were conducted on untreated and treated fabrics according to ASTM D6413-08. An Automatic Vertical Flammability Cabinet model VC-2 made by Govmark (Farmingdale, NY) was used to conduct vertical flame testing.

RESULTS AND DISCUSSION

Film Growth. The influence of the deposition mixture pH on the resulting film thickness was evaluated using ellipsometry. A series of films were prepared with various BPEI solution pHs, keeping the Laponite solution at its unadjusted pH of 10.1. Figure 2a shows that these films exhibit linear growth, and Table 1 shows that films made with lower BPEI pH are thinner than those prepared at higher pH. Owing to its protonatable secondary and tertiary amine backbones and primary amine side chains, BPEI has a greater positive charge density at lower pH. It is for this reason that BPEI has stronger electrostatic adsorption with negatively charged substrates and clay, making it lie relatively flat and resulting in thinner films. A separate series of films was made, varying the pH of the Laponite solution and keeping BPEI at its unadjusted pH of 10.3, to see if a similar variation in the film growth would result. In this case, linear growth that varied with the pH was again observed (Figure 2b), but films are thicker at lower Laponite pH. In the system where Laponite is at pH 6, it may actually be forming a "house-of-cards" structure because its edges are positively charged, which promotes edge-to-face associations (45, 46). The locally high clay concentration at the surface of the thin film could lead to gelation and ultimately to some type of collapsed house-of-cards structure, which would explain the thicker deposition observed at pH 6 in Figure 2b.

To further explore these structural mechanisms of film growth, another series of experiments was performed by adding salt into either the BPEI or Laponite solutions. Because of the charge-screening effect of the salt (47), the addition of increasing sodium chloride concentrations to the BPEI deposition solutions (at pH 8) resulted in the formation of thicker films, as shown in Figure 3. In the case of an unadjusted BPEI solution and Laponite suspensions (independent of the pH), the thickness of the films is nearly unaffected by the salt concentration (data not shown). Compositional information was obtained by a QCM, which measured the weight of each deposited layer. From the data shown in Figure 4 and Table 2, films of unadjusted BPEI and pH 6 Laponite appear to have the highest density and Laponite percentage, suggesting that stacks of Laponite platelets were deposited on the substrate surface during each coating cycle when the clay is at pH 6. When BPEI/Laponite

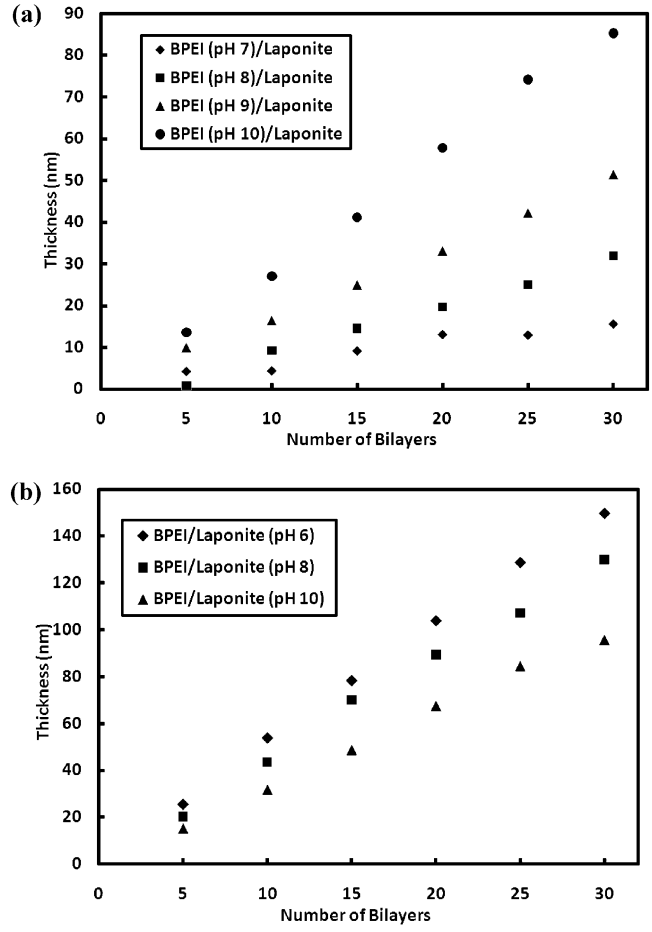

FIGURE 2. Film thickness as a function of the number of BLs deposited for LbL assemblies made with various BPEI (a) and Laponite (b) deposition mixture pHs. Only one ingredient's pH was varied at a time, while the other was held at its unadjusted pH (10.3 for BPEI and 10.1 for Laponite).

Table 1. Thickness per BL for Various BPEI/Laponite Recipes

LbL system	nm per BL cycle	LbL system	nm per BL cycle
BPEI (pH 7)/Laponite	0.52	BPEI/Laponite	2.99
BPEI (pH 8)/Laponite	1.06	BPEI/Laponite (pH 6)	4.99
BPEI (pH 9)/Laponite	1.71	BPEI/Laponite (pH 8)	4.33
BPEI (pH 10)/Laponite	2.84	BPEI/Laponite (pH 10)	3.19

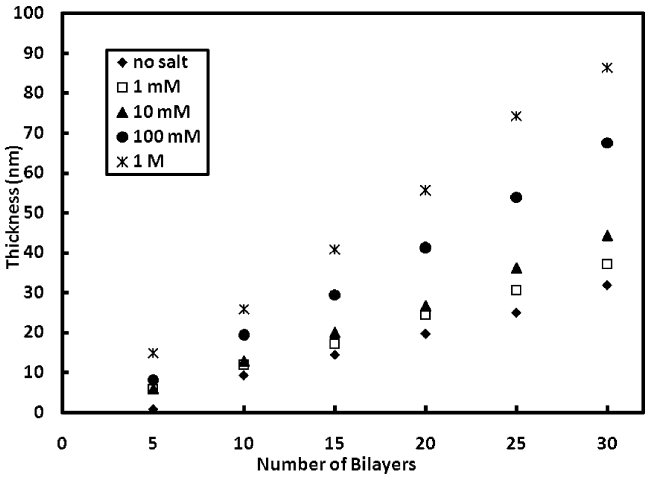

FIGURE 3. BPEI/Laponite film thickness as a function of BLs deposited with various NaCl concentrations. The BPEI solution was maintained at pH 8, and the Laponite pH was unadjusted.

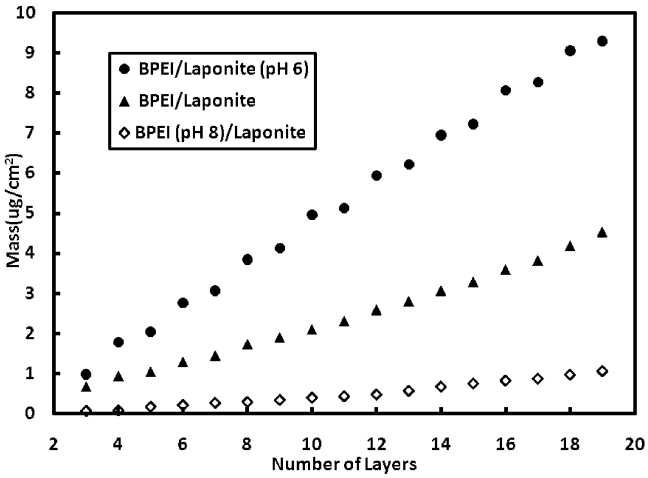

FIGURE 4. Film mass as a function of layers deposited for three different BPEI/Laponite systems. In all cases, BPEI is odd layers and Laponite is even layers. When no pH is specified for BPEI or Laponite, it means the unadjusted pH was used.

Table 2. Film Density and Composition for Various BPEI/Laponite Recipes

LbL system	density (g/cm^3)	BPEI (wt %)	Laponite (wt %)
BPEI (pH 8)/Laponite	1.42	31 ± 14	69 ± 14
BPEI/Laponite	1.61	38 ± 7	62 ± 20
BPEI/Laponite (pH 6)	1.91	17 ± 9	83 ± 7

(pH 6) is compared with other BPEI/Laponite films at higher Laponite pH (see Table 1), not only are the BLs thicker, but the weight percentage of Laponite is higher as well when using lower-pH Laponite (see Table 2).

Film Structure. Figure 5 shows TEM cross sections of three sample films, made with different BPEI and Laponite pH conditions. These 30-BL films were deposited on PS substrates to facilitate sectioning. The BLs of the BPEI (pH 10)/Laponite film (Figure 5a) are clearly thicker than those of the BPEI (pH 8)/Laponite film (Figure 5b). The BPEI/Laponite (pH 6) film (Figure 5c) appears to have a cross-sectional microstructure different from that the other two films, which could be further evidence of somewhat collapsed edge-to-face associations (i.e., house-of-cards). Several light-colored round or elliptical areas appear in the lateral view of this cross section (pointed out by arrows) that correspond to the size of Laponite platelets tilted on their sides. In the same image (Figure 5c), the outline of "standing" clay platelets on the film surface is clearly visible (topmost arrow), unlike what is observed in Figure 5a,b. The thicknesses of the films in these images correlate well with the ellipsometry data shown in Figure 2. All of the films appear wavy in the images, which may be caused by stress relaxation in the film during sectioning with a diamond knife and/or because of the tilted layers of clay (48).

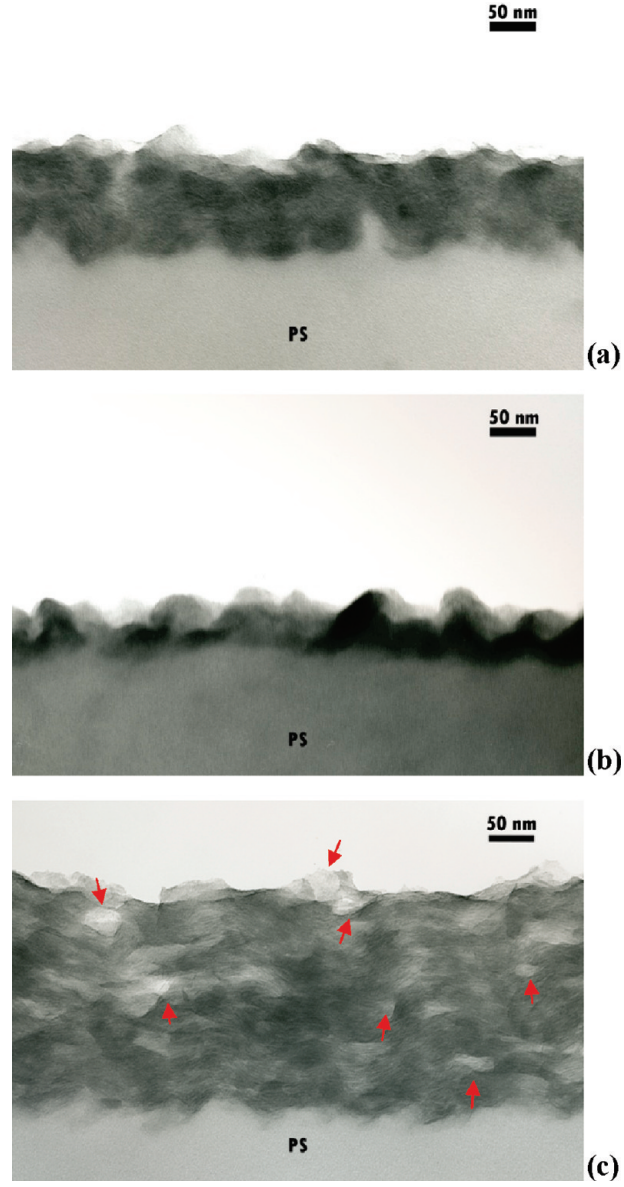

FIGURE 5. TEM cross-sectional images of 30-BL assemblies made with Laponite and BPEI at pH 10 (a) and pH 8 (b) and with BPEI and Laponite at pH 6 (c).

Tapping-mode AFM was used to characterize the surfaces of 10-BL films because at this number of layers a maximum roughness was reached in similar films (Laponite/PDDA) (35). Figure 6 shows height and phase images of a 10-BL BPEI (pH 7)/Laponite film. At lower magnification (Figure 6a,b), the surface resembles a cobblestone path that is uniformly

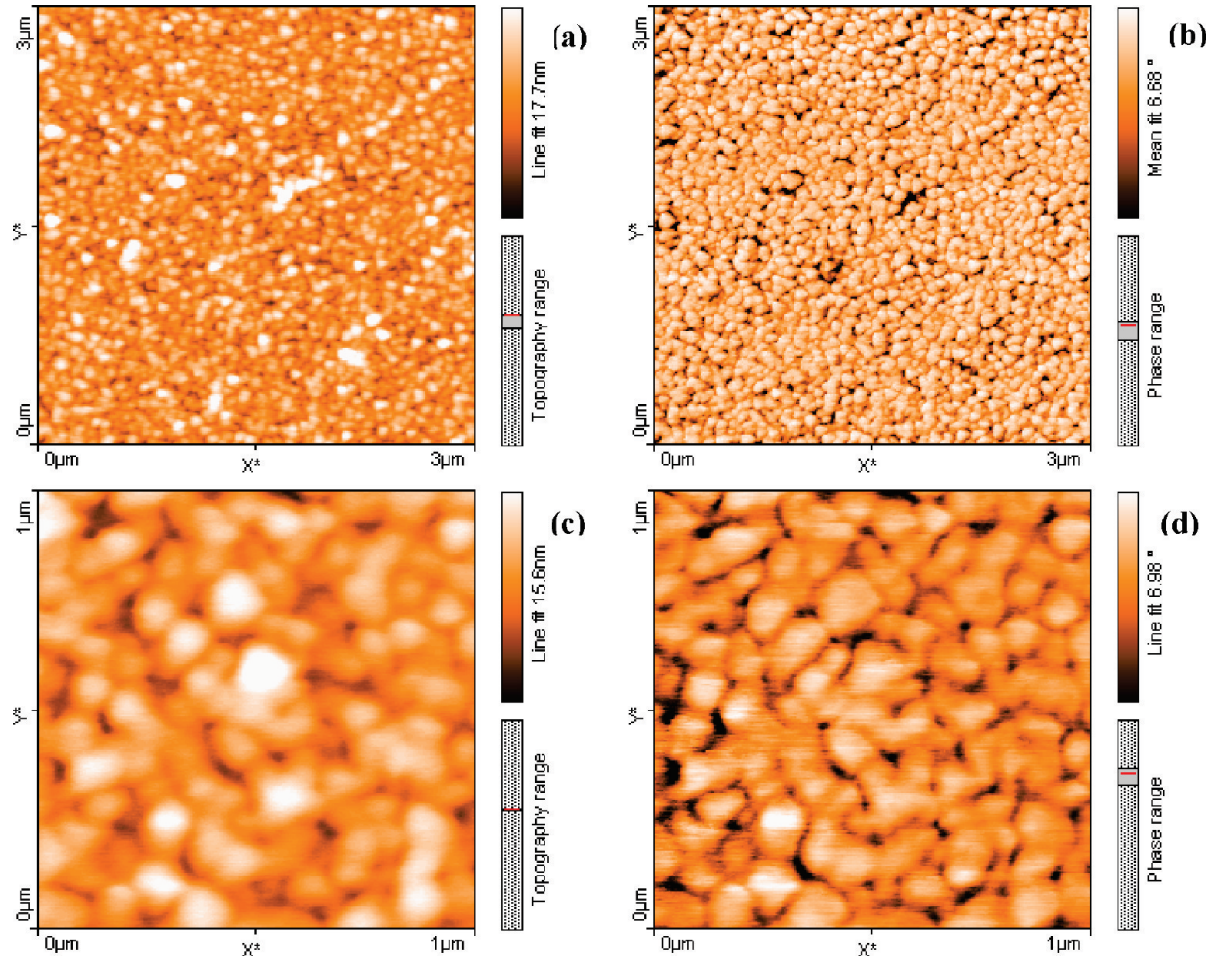

FIGURE 6. AFM height (a and c) and phase (b and d) surface images of a 10-BL BPEI (pH 7)/Laponite film; (a and b) under 3 μm scale; (c and d) under 1 μm scale.

covered by clay platelets whose largest dimension is oriented parallel to the silicon wafer substrate. The size of the clay platelets looks uniform from these images, and the surface texture is similar in all LbL films deposited with unadjusted Laponite (pH 10.1) and various BPEI pHs. A slightly different structure is observed on the surface of a film made with unadjusted BPEI (pH 10.3) and Laponite at pH 6 (see the Supporting Information), but the surface roughness is similar for all films. The root-mean-square roughness of BPEI (pH 7)/Laponite is 2.5 nm, while it is 2.2 nm for BPEI (pH 10)/Laponite and 2.6 nm for BPEI/Laponite (pH 6) when using a 20 μm square area.

Figure 7 shows patterns from XRD performed on a neat Laponite powder and four LbL films made with various pH conditions. Neat clay powder shows the major characteristic peaks that are consistent with those reported in the literature (40, 49). The low-angle peak at 6.8° derives from a basal spacing of 13.0 Å, which is the periodic distance from platelet to platelet. Because the thickness of each platelet is 1 nm, the distance between platelets is 3 Å. In all four films, the low-angle peaks shift to ~6.3°, which means that the distance between platelets increases to about 4 Å. From these results, it appears that the clay platelets exhibit lamellar stacking (50), with at least two layers of Laponite deposited per coating cycle. On the basis of AFM surface images

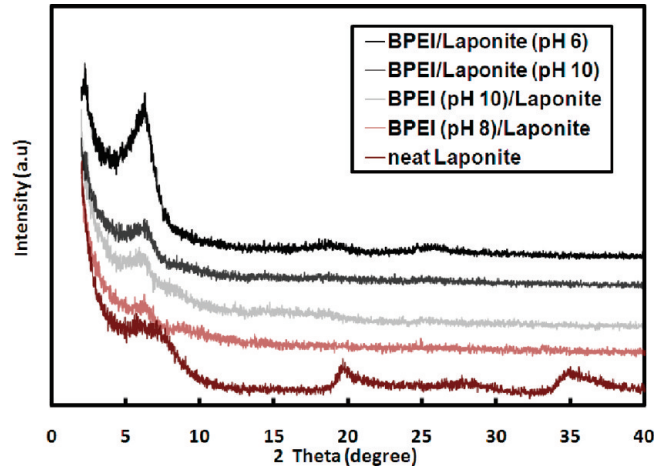

FIGURE 7. XRD patterns for neat Laponite and 30-BL films made by varying the pH of the BPEI and Laponite solutions.

(see Figure 2 and the Supporting Information), the films likely have ordering in the *z* direction, which agrees well with other studies of clay-based assemblies (40, 48).

The BPEI/Laponite (pH 6) system exhibits the most pronounced low-angle peak (~6.3°) in Figure 7. The weight of each clay deposition, measured with a QCM (not shown), suggests that each clay deposition is approximately 3.6 nm thick (assuming a planar packing density of 0.9), which

translates to four stacked platelets. In the TEM image shown previously (Figure 5c), it can be seen that this film is mostly arranged as lamellar layers, but the tilted clay platelets suggest a collapsed "house-of-cards" structure (45, 46). When the pH of Laponite suspensions is reduced with HCl, the H^+ ions also diminish the negative surface charge by attaching to the face of Laponite (51). This combination of edge-to-face attractions and charge screening is believed to allow more Laponite to be adsorbed onto the assembly surface in each dipping cycle. This provides a possible explanation for the thicker growth observed for BPEI/Laponite (pH 6). None of the other systems studied exhibits such a thick growth and evidence of tilted platelets.

Mechanical Behavior. The hardness and reduced moduli of BPEI/Laponite assemblies were determined using nanoindentation, in which a force is applied to an indenter probe while continuously measuring the applied force (P) and the probe displacement (h). Figure 8a shows two example indents, one on a relatively thin film and the other on a thicker film. The peak load of indentation was 2 μN for all films, except BPEI (pH 8)/Laponite, which was 5 μN. The hardness (H) is defined as the ratio of the maximum load (P_{max}) to the projected contact area (A), shown in eq 1.

$$H = \frac{P_{max}}{A} \quad (1)$$

The reduced modulus (E_r) is defined in eq 2, where S, the unloading stiffness, is defined by eq 3.

$$E_r = \frac{S\sqrt{\pi}}{2\sqrt{A}} \quad (2)$$

$$S = \frac{dP}{dh} \quad (3)$$

Parts b and c of Figure 8 show these two mechanical properties for 40-BL films made with BPEI and Laponite at various pHs. The results indicate that the thinnest film [BPEI (pH 8) and unadjusted Laponite] exhibits the highest reduced modulus, which is proportional to the stiffness (the initial slope of the unloading curve) and the same as the elastic modulus to a first approximation (52). This may be due to a substrate effect because the film is only 40 nm thick and the indentation depth was more than 10% of this value. However, examination of the load–displacement curves (Figure 8a) reveals that this film is stiffer even during the initial

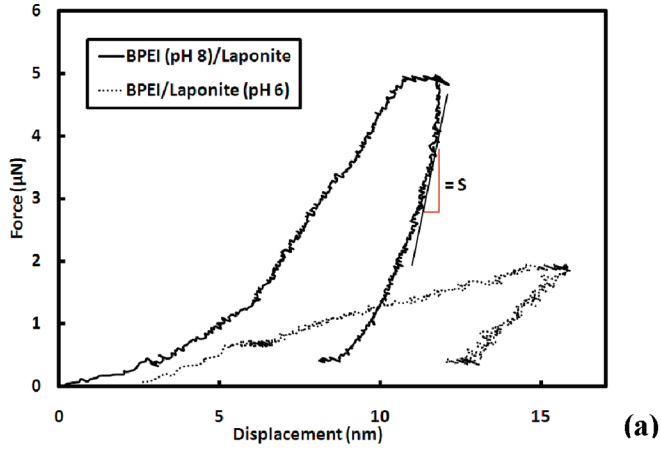

(a)

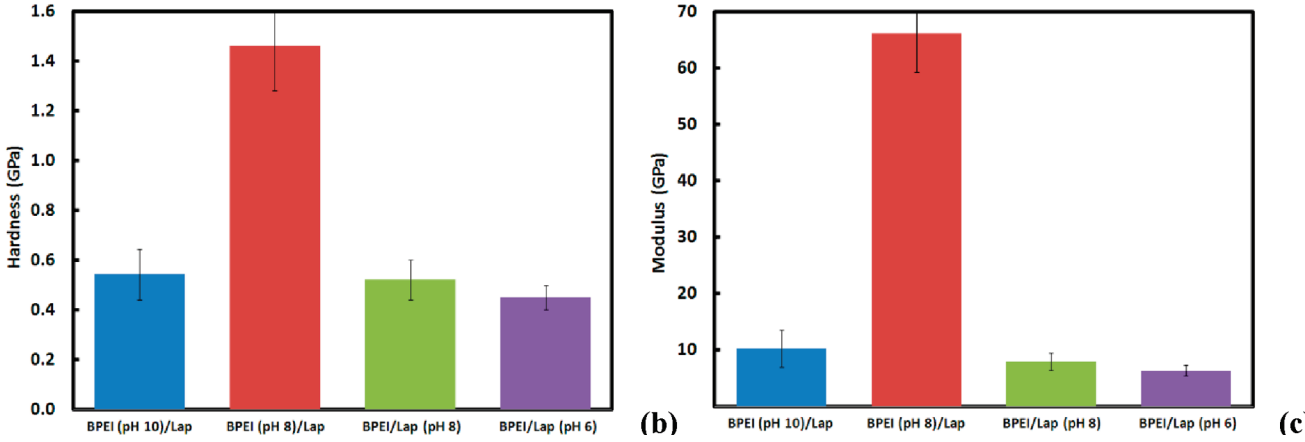

(b) (c)

FIGURE 8. Load–displacement curves (a) and the mechanical properties [(b) hardness and (c) elastic modulus] of 40-BL thin films.

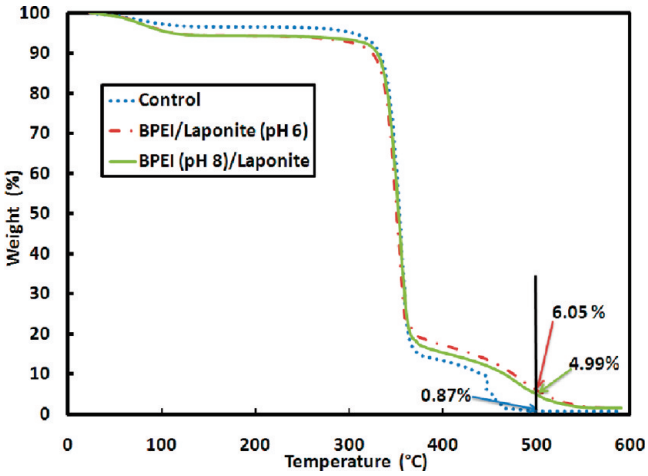

FIGURE 9. Weight loss as a function of the temperature for cotton fabrics coated with 10 BLs of BPEI at BPEI/Laponite (pH 6) and BPEI (pH 8)/Laponite. These results were obtained using TGA at a heating rate of 20 °C/min.

loading segment, which indicates a higher modulus even before the onset of any substrate effect. The other three films have thicknesses above 100 nm and exhibit a hardness of 0.5 ± 0.05 GPa with 10% indentation depth, which is in agreement with those working with similar systems (33).

The reduced modulus is related to the modulus of elasticity (E) through eq 4.

$$\frac{1}{E_r} = \frac{1 - \nu_i^2}{E_i} + \frac{1 - \nu_s^2}{E_s} \qquad (4)$$

where the subscript i corresponds to the indenter material, the subscript s refers to the indented sample material, and ν is Poisson's ratio. For a diamond indenter probe, E_i is 1,140 GPa, which is a huge number compared to the substrate's modulus, so the reduced modulus of the film is very close to its modulus of elasticity. Even though the film made with unadjusted BPEI and Laponite at pH 6 has a greater concentration of clay (see Table 2), the hardness and modulus are lower than those for the other three films. This is probably because it experiences less substrate effect when the mechanical properties are measured. Nevertheless, the modulus and hardness values of the LbL thin films made with polymer and clay are relatively higher than those of pure polymer (e.g., PDDA) films (48). Because of the high transparency and good mechanical properties achieved in these nanocomposite thin films, this simple process could be used as a hard coating for plastic substrates, as an alternative to the sol–gel technique (53, 54).

Flame Resistance for Fabric. Many researchers have shown that clay imparts flame resistance to bulk polymers (55–57). Others have shown that polymer/clay LbL self-assembly can be applied on paper (30) and wood fibers (58). Poly(allylamine hydrochloride) and Kaolin clay coatings on paper were shown to change the wettability of the paper from hydrophilic to hydrophobic (30). PDDA- and MMT-coated wood fibers were observed to attain increased thermal stability relative to the unmodified material tested by thermogravimetric analysis (TGA) (58). At present, no literature shows the application of the LbL coating on cotton fabrics, especially for the purpose of flame suppression. Fabric samples were coated with 10 BLs of BPEI (pH 8)/Laponite and BPEI/Laponite (pH 6), which resulted in less than a 2% increase in the fabric weight. At 500 °C, under an air atmosphere, the uncoated fabric left less than 0.9 wt % residue, as shown in Figure 9. The char weight percentages for the coated fabrics were much higher and very close to each other (5 and 6 wt %) for the two different coatings.

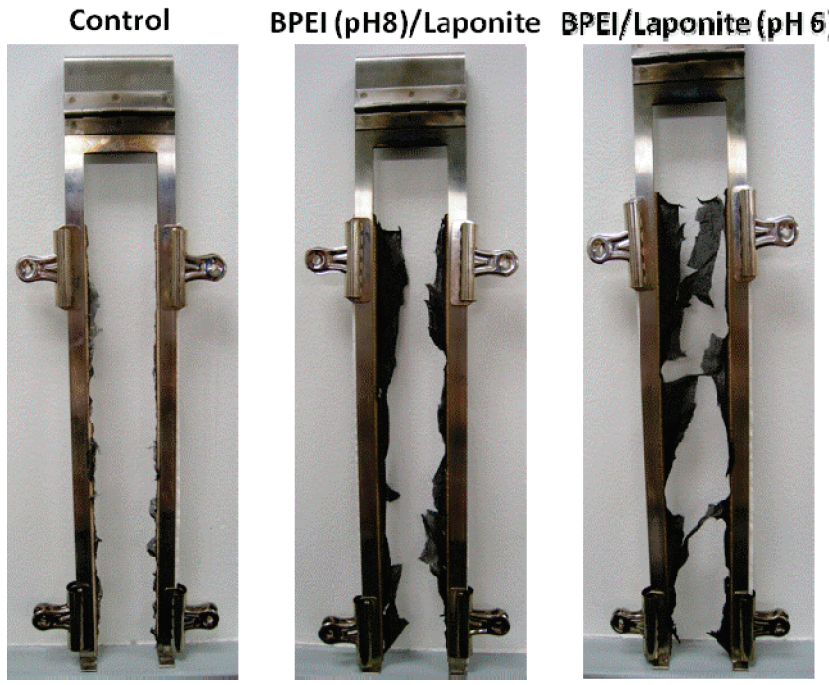

FIGURE 10. Images of uncoated and coated cotton fabrics following the vertical flame test. The coated fabric is 10 BLs of a given recipe.

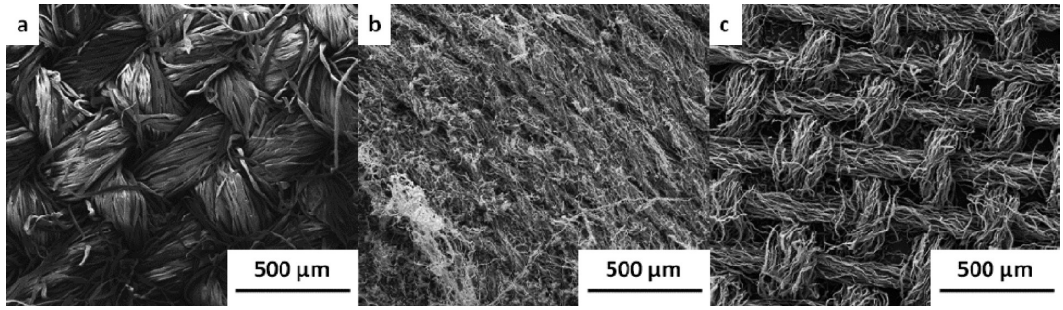

FIGURE 11. SEM images of virgin fabric before (a) and after (b) flame testing; (c) coated fabric after flame testing [BPEI (pH 8)/Laponite].

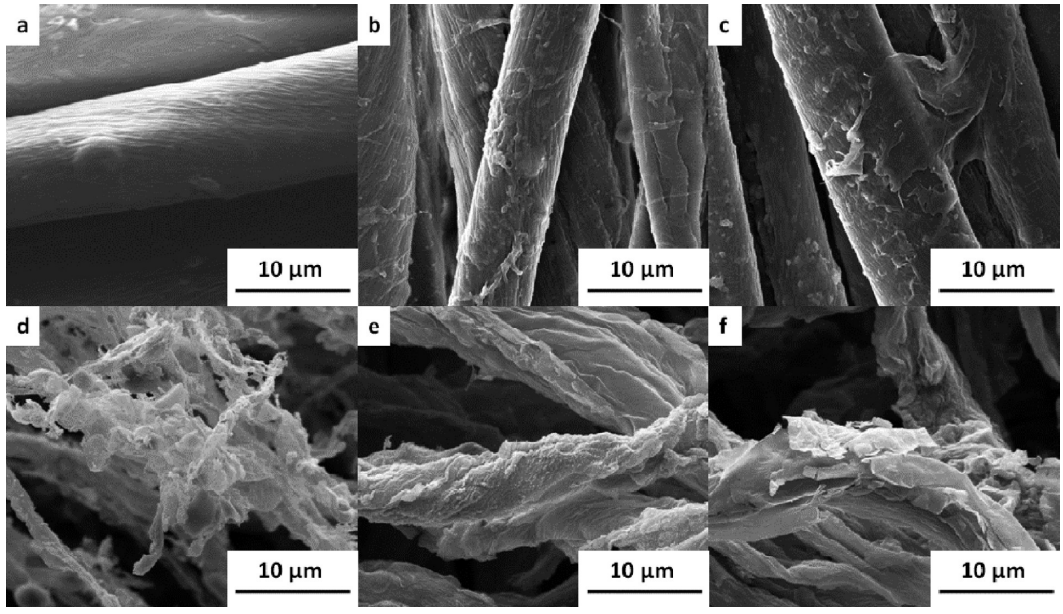

FIGURE 12. SEM images of fabrics before (a–c) and after (d–f) flame testing: (a and d) uncoated fabrics; (b and e) fabric coated with 10 BLs of BPEI (pH 8)/Laponite; (c and f) fabric coated with 10 BLs of BPEI/Laponite (pH 6).

It seems that the clay coating delays the degradation of the cotton by providing a sheathlike ceramic barrier.

Equivalently coated fabrics were put through vertical flame testing (ASTM D6413). A more vigorous flame was observed on the control fabric compared to the coated fabrics (see the Supporting Information). Additionally, there was more afterglow on the control fabric. These three treatments showed similar ignition and afterflame times, but the afterglow times for coated fabrics were 8–10 s less than those for the uncoated fabric. After burning, no control fabric was left on the sample holder, but the two coated fabrics left significant char, as shown in Figure 10. All of the fabrics were examined by SEM, before and after flame testing. The control fabrics left only ashes after flame exposure, so the ashes were used as SEM samples in those cases. Under lower magnification, the weave of the fabric can be clearly seen in Figure 11a. After flame testing, the ash from the uncoated fabric (Figure 11b) and the char from coated fabric (Figure 11c) were examined under the same magnification. The weave structure of the char from coated fabrics is still relatively intact, but the threads of the char shrank after flame testing, leaving gaps between the threads.

Before flame testing, the fiber surface in the control fabric (Figure 12a) appears to be very clean and smooth compared to that of the coated fabrics (Figure 12b,c). The aggregated Laponite particles can be seen on the fibers of the coated fabrics. Each fiber of the fabric was at least partially, if not completely, covered by the clay coating. After flame testing, the char was again imaged. Because the control fabric was burned completely, its ashes were taken from the edge of the vertical flame sample holder for imaging. Broken pieces and holes in the fiber strands of the control fabric, caused by burning (Figure 12d), as well as some fibrous residues that are no longer the original fabric fibers, can be seen very clearly in the SEM images. In the case of the char from the coated fabrics, a solid shield layer on the fibers can be seen clearly in Figure 12e,f. It is possible that, during burning at high temperature, the Laponite clay platelets sintered together could account for not seeing aggregated Laponite or the edges of the platelets but large continuous pieces of coating instead. There is no question that significant degradation occurs even in the coated fabric, but this work provides some initial evidence that clay-based assemblies may be an interesting alternative to current flame suppression technologies for fibers and fabrics.

CONCLUSIONS

The growth, structure, and mechanical behavior of LbL thin films, composed of the weak polyelectrolyte polyethylenimine and Laponite clay, were studied. The film thickness per BL can be tuned from 0.5 to 5 nm by altering pH of the aqueous deposition solutions. The thickest films are achieved with unadjusted BPEI (pH 10.3) and pH 6 Laponite. AFM images show very uniform film surfaces and a highly ordered polymer/clay assembly in all of the BPEI/Laponite systems. Tilted clay platelets can be seen in TEM cross-sectional images of the film made with unadjusted BPEI and pH 6 Laponite, which could be a collapsed house-of-cards structure that consists of edge-to-face assocations. Nonetheless, XRD shows that the gallery spacing in the lamellar structure is the same for films made using different BPEI and Laponite pH values. At 40 BLs, these films have a hardness of 0.5 GPa and reduced moduli of 6−10 GPa, depending on recipe. This type of thin-film system may be useful for ion (charge) transport (40) and protective layers (e.g., hard coating or flame resistance). These assemblies can be directly applied to cotton fabric, and that results in a significant improvement in the thermal stability. SEM images show that LbL coating three-dimensionally coats the surface of each individual thread of the fabric and provides some flame suppression. This concept could be further developed to impart flame-retardant behavior to clothing and other materials for fire safety applications (e.g., soft furnishings). Additional coating systems, using other clays and nanoparticles, are currently being evaluated for improved performance.

Acknowledgment. The authors acknowledge the Building and Fire Research Laboratory at the National Institute of Standards and Technology for financial support of this work. We also thank Charlene M. Dvoracek for assistance with TEM imaging and Dr. Yeon Seok Kim for assistance with SEM imaging.

Supporting Information Available: Images of vertical flame tests for uncoated and coated fabrics. This material is available free of charge via the Internet at http://pubs.acs.org.

REFERENCES AND NOTES

(1) Ariga, K.; Hill, J. P.; Ji, Q. *Phys. Chem. Chem. Phys.* **2007**, *9*, 2319–2340.
(2) Decher, G.; Schlenoff, J. B. *Multilayer thin films: sequential assembly of nanocomposite materials*; Wiley-VCH: New York, 2003; p xix, 524p.
(3) Bertrand, P.; Jonas, A.; Laschewsky, A.; Legras, R. *Macromol. Rapid Commun.* **2000**, *21*, 319–348.
(4) Shimazaki, Y.; Mitsuishi, M.; Ito, S.; Yamamoto, M. *Langmuir* **1997**, *13*, 1385–1387.
(5) Shimazaki, Y.; Mitsuishi, M.; Ito, S.; Yamamoto, M. *Langmuir* **1998**, *14*, 2768–2773.
(6) Shimazaki, Y.; Nakamura, R.; Ito, S.; Yamamoto, M. *Langmuir* **2001**, *17*, 953–956.
(7) Bergbreiter, D. E.; Tao, G. L.; Franchina, J. G.; Sussman, L. *Macromolecules* **2001**, *34*, 3018–3023.
(8) Lv, F.; Peng, Z. H.; Zhang, L. L.; Yao, L. S.; Liu, Y.; Xuan, L. *Liq. Cryst.* **2009**, *36*, 43–51.
(9) Sun, J. Q.; Wu, T.; Liu, F.; Wang, Z. Q.; Zhang, X.; Shen, J. C. *Langmuir* **2000**, *16*, 4620–4624.
(10) Bergbreiter, D. E.; Chance, B. S. *Macromolecules* **2007**, *40*, 5337–5343.
(11) Mermut, O.; Barrett, C. J. *J. Phys. Chem. B* **2003**, *107*, 2525–2530.
(12) Sui, Z. J.; Salloum, D.; Schlenoff, J. B. *Langmuir* **2003**, *19*, 2491–2495.
(13) Tan, H. L.; McMurdo, M. J.; Pan, G. Q.; Van Patten, P. G. *Langmuir* **2003**, *19*, 9311–9314.
(14) Chang, L.; Kong, X.; Wang, F.; Wang, L.; Shen, J. *Thin Solid Films* **2008**, *516*, 2125–2129.
(15) Zhang, H. N.; Ruhe, J. *Macromolecules* **2003**, *36*, 6593–6598.
(16) McAloney, R. A.; Sinyor, M.; Dudnik, V.; Goh, M. C. *Langmuir* **2001**, *17*, 6655–6663.
(17) Shiratori, S. S.; Rubner, M. F. *Macromolecules* **2000**, *33*, 4213–4219.
(18) Fu, J. H.; Ji, J.; Fan, D. Z.; Shen, J. C. *J. Biomed. Mater. Res. A* **2006**, *79A*, 665–674.
(19) Dvoracek, C. M.; Sukhonosova, G.; Benedik, M. J.; Grunlan, J. C. *Langmuir* **2009**, *25*, 10322–10328.
(20) Hiller, J.; Mendelsohn, J. D.; Rubner, M. F. *Nat. Mater.* **2002**, *1*, 59–63.
(21) Choi, K.; Yoo, S. J.; Sung, Y. E.; Zentel, R. *Chem. Mater.* **2006**, *18*, 5823–5825.
(22) DeLongchamp, D. M.; Hammond, P. T. *Chem. Mater.* **2004**, *16*, 4799–4805.
(23) Jain, V.; Sahoo, R.; Jinschek, J. R.; Montazami, R.; Yochum, H. M.; Beyer, F. L.; Kumar, A.; Heflin, J. R. *Chem. Commun.* **2008**, 3663–3665.
(24) Yu, H. H.; Cao, T.; Zhou, L. D.; Gu, E. D.; Yu, D. S.; Jiang, D. S. *Sens. Actuators, B* **2006**, *119*, 512–515.
(25) Everett, W. N.; Jan, C. J.; Sue, H. J.; Grunlan, J. C. *Electroanalysis* **2007**, *19*, 964–972.
(26) Aoki, P. H. B.; Volpati, D.; Riul, A.; Caetano, W.; Constantino, C. J. L. *Langmuir* **2009**, *25*, 2331–2338.
(27) Jang, W. S.; Rawson, I.; Grunlan, J. C. *Thin Solid Films* **2008**, *516*, 4819–4825.
(28) Tang, Z. Y.; Wang, Y.; Podsiadlo, P.; Kotov, N. A. *Adv. Mater.* **2006**, *18*, 3203–3224.
(29) Ras, R. H. A.; Umemura, Y.; Johnston, C. T.; Yamagishi, A.; Schoonheydt, R. A. *Phys. Chem. Chem. Phys.* **2007**, *9*, 918–932.
(30) Ou, R. Q.; Zhang, J. G.; Deng, Y. L.; Ragauskas, A. J. *J. Appl. Polym. Sci.* **2007**, *105*, 1987–1992.
(31) Mehta, G.; Kiel, M. J.; Lee, J. W.; Kotov, N.; Linderman, J. J.; Takayama, S. *Adv. Funct. Mater.* **2007**, *17*, 2701–2709.
(32) Podsiadlo, P.; Kaushik, A. K.; Arruda, E. M.; Waas, A. M.; Shim, B. S.; Xu, J. D.; Nandivada, H.; Pumplin, B. G.; Lahann, J.; Ramamoorthy, A.; Kotov, N. A. *Science* **2007**, *318*, 80–83.
(33) Podsiadlo, P.; Michel, M.; Lee, J.; Verploegen, E.; Kam, N. W. S.; Ball, V.; Lee, J.; Qi, Y.; Hart, A. J.; Hammond, P. T.; Kotov, N. A. *Nano Lett.* **2008**, *8*, 1762–1770.
(34) Kleinfeld, E. R.; Ferguson, G. S. *Chem. Mater.* **1995**, *7*, 2327–2331.
(35) van Duffel, B.; Schoonheydt, R. A.; Grim, C. P. M.; De Schryver, F. C. *Langmuir* **1999**, *15*, 7520–7529.
(36) Glinel, K.; Laschewsky, A.; Jonas, A. M. *J. Phys. Chem. B* **2002**, *106*, 11246–11252.
(37) Malwitz, M. M.; Lin-Gibson, S.; Hobbie, E. K.; Butler, P. D.; Schmidt, G. *J. Polym. Sci., Part B: Polym. Phys.* **2003**, *41*, 3237–3248.
(38) Vuillaume, P. Y.; Glinel, K.; Jonas, A. M.; Laschewsky, A. *Chem. Mater.* **2003**, *15*, 3625–3631.
(39) Lee, H. C.; Lee, T. W.; Kim, T. H.; Park, O. O. *Thin Solid Films* **2004**, *458*, 9–14.
(40) Lutkenhaus, J. L.; Olivetti, E. A.; Verploegen, E. A.; Cord, B. M.; Sadoway, D. R.; Hammond, P. T. *Langmuir* **2007**, *23*, 8515–8521.
(41) Thompson, D. W.; Butterworth, J. T. *J. Colloid Interface Sci.* **1992**, *151*, 236–243.
(42) Cummins, H. Z. *J. Non-Cryst. Solids* **2007**, *353*, 3891–3905.
(43) Owens, D. K. *J. Appl. Polym. Sci.* **1975**, *19*, 3315–3326.
(44) Zhang, D.; Sun, Q.; Wadsworth, L. C. *Polym. Eng. Sci.* **1998**, *38*, 965–970.
(45) Diz, H. M. M.; Rand, B. *Br. Ceram. Trans. J.* **1989**, *88*, 162–166.
(46) Saunders, J. M.; Goodwin, J. W.; Richardson, R. M.; Vincent, B. *J. Phys. Chem. B* **1999**, *103*, 9211–9218.
(47) Schoeler, B.; Kumaraswamy, G.; Caruso, F. *Macromolecules* **2002**, *35*, 889–897.
(48) Vertlib, V.; Dietiker, M.; Plotze, M.; Yezek, L.; Spolenak, R.; Puzrin, A. M. *J. Mater. Res.* **2008**, *23*, 1026–1035.

(49) Le Luyer, C.; Lou, L.; Bovier, C.; Plenet, J. C.; Dumas, J. G.; Mugnier, J. *Opt. Mater.* **2001**, *18*, 211–217.
(50) Kehlbeck, J. D.; Hagerman, M. E.; Cohen, B. D.; Eliseo, J.; Fox, M.; Hoek, W.; Karlin, D.; Leibner, E.; Nagle, E.; Nolan, M.; Schaefer, I.; Toney, A.; Topka, M.; Uluski, R.; Wood, C. *Langmuir* **2008**, *24*, 9727–9738.
(51) Pawar, N.; Bohidar, H. B. *Colloids Surf., A* **2009**, *333*, 120–125.
(52) Oliver, W. C.; Pharr, G. M. *J. Mater. Res.* **1992**, *7*, 1564–1583.
(53) Sepeur, S.; Kunze, N.; Werner, B.; Schmidt, H. *Thin Solid Films* **1999**, *351*, 216–219.
(54) Wu, L. Y. L.; Soutar, A. M.; Zeng, X. T. *Surf. Coat. Technol.* **2005**, *198*, 420–424.
(55) Gilman, J. W.; Harris, R. H.; Shields, J. R.; Kashiwagi, T.; Morgan, A. B. *Polym. Adv. Technol.* **2006**, *17*, 263–271.
(56) Gui, H.; Zhang, X. H.; Liu, Y. Q.; Dong, W. F.; Wang, Q. G.; Gao, J. M.; Song, Z. H.; Lai, J. M.; Qiao, J. L. *Compos. Sci. Technol.* **2007**, *67*, 974–980.
(57) Camino, G.; Tartaglione, G.; Frache, A.; Manferti, C.; Costa, G. *Polym. Degrad. Stab.* **2005**, *90*, 354–362.
(58) Lin, Z. Y.; Renneckar, S.; Hindman, D. P. *Cellulose* **2008**, *15*, 333–346.

AM900484Q